Low Voltage Electron Microscopy

Principles and Applications

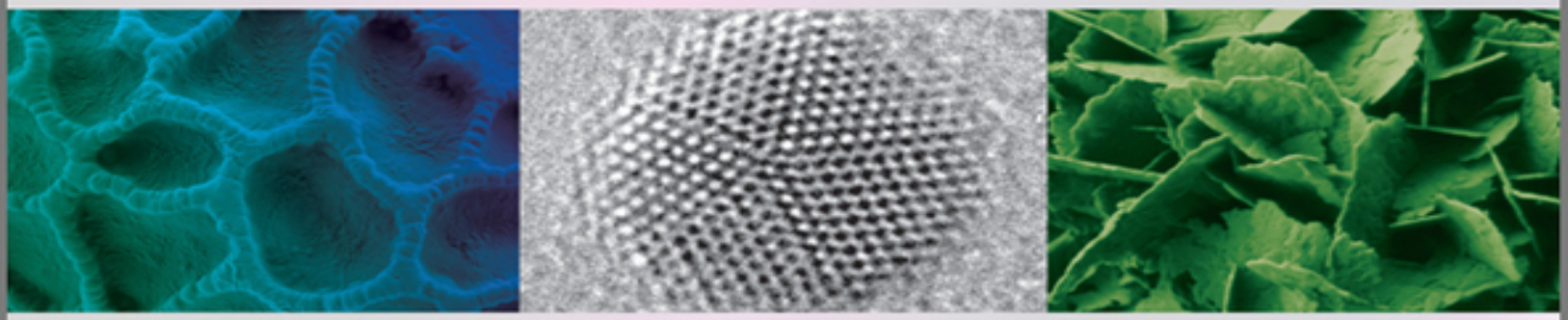

Editors
David C. Bell and Natasha Erdman

WILEY

RMS

Table of Contents

Current and future titles in the Royal Microscopical Society— John Wiley Series

Published

Principles and Practice of Variable Pressure/Environmental Scanning Electron Microscopy (VP-ESEM)

Debbie Stokes

Aberration-Corrected Analytical Electron Microscopy

Edited by Rik Brydson

Diagnostic Electron Microscopy— A Practical Guide to Interpretation and Technique

Edited by John W. Stirling, Alan Curry & Brian Eyden

Low Voltage Electron Microscopy— Principles and Applications

Edited by David C. Bell & Natasha Erdman

Forthcoming

Atlas of Images and Spectra for Electron Microscopists

Edited by Ursel Bangert

Understanding Practical Light Microscopy

Jeremy Sanderson

Focused Ion Beam Instrumentation: Techniques and Applications

Dudley Finch & Alexander Buxbaum

Electron Beam-Specimen Interactions and Applications in Microscopy

Budhika Mendis

Low Voltage Electron Microscopy: Principles and Applications

Edited by

David C. Bell
Harvard University, USA

and

Natasha Erdman
JEOL USA Inc., USA

Published in association with the Royal Microscopical Society

Series Editor: Susan Brooks

A John Wiley & Sons, Ltd., Publication

This edition first published 2013

Registered office

John Wiley & Sons Ltd, The Atrium, Southern Gate, Chichester, West Sussex, PO19 8SQ, United Kingdom

For details of our global editorial offices, for customer services and for information about how to apply for permission to reuse the copyright material in this book please see our website at www.wiley.com.

Library of Congress Cataloging-in-Publication Data

Low voltage electron microscopy : principles and applications / edited by David C. Bell, Natasha Erdman.

pages cm.

Includes index.

ISBN 978-1-119-97111-5 (hardback)

1. Electron microscopy– Technique. I. Bell, D. C. (David C.) II. Erdman, Natasha.

QH212.E4L69 2012

502.8$′25– dc23

2012033919

A catalogue record for this book is available from the British Library.

HB ISBN: 978-1-119-97111-5

List of Contributors

David C. Bell, School of Engineering and Applied Sciences, Harvard University, Cambridge, MA 02134, USA

Matthew F. Chisholm, Materials Science and Technology Division, Oak Ridge National Laboratory, Oak Ridge, TN 37831, USA

Niklas Dellby, Nion Co., Kirkland, WA 98033, USA

Natasha Erdman, JEOL USA Inc., Peabody, MA 01960, USA

Alexander Henstra, FEI Company, Building AAE, PO Box 80066, 5600 KA Eindhoven, The Netherlands

Juan Carlos Idrobo, Materials Science and Technology Division, Oak Ridge National Laboratory, Oak Ridge, TN 37831, USA

Robert Klie, Nanoscale Physics Group, Department of Physics, University of Illinois at Chicago, Chicago, IL 60607, USA

Ondrej L. Krivanek, Nion Co., Kirkland, WA 98033, USA

Tracy C. Lovejoy, Nion Co., Kirkland, WA 98033, USA

Quentin M. Ramasse, SuperSTEM Laboratory, STFC Daresbury, Daresbury, WA4 4AD, UK

Lubomir Tuma, FEI Company, Czech Republic s.r.o. Podnikatelska 2, 612 00 Brno, Czech Republic

Gerard N.A. van Veen, FEI Company, Building AAE, PO Box 80066, 5600 KA Eindhoven, The Netherlands

Richard J. Young, FEI Company, 5350 NE Dawson Creek Drive, Hillsboro OR 97124, USA

Wu Zhou, Department of Physics & Astronomy, Vanderbilt University, Nashville, TN 37235, USA and Materials Science and Technology Division, Oak Ridge National Laboratory, Oak Ridge, TN 37831, USA

Preface

The introduction of the electron microscope in the 1930s enabled the visual confirmation that virus particles actually existed for the first time and were separate individual “living” entities. The new technology advances of electron microscopes at that time period, in particular those manufactured by Siemens in Germany and the Radio Corporation of America (RCA) enabled the routine imaging of biological tissues and cells. Further advances allowed the detailed identification and characterization of viruses, as better techniques and more powerful microscopes were developed. Electron microscopic imaging was now in a dramatic new way completely beyond the capabilities of light microscopy.

The electron microscope was invented by Max Knoll and Ernst Ruska in 1931, although there were many researchers working on the development of electron microscopes. Ernst Ruska was awarded half of the Nobel Prize for Physics in 1986 for his invention. (The other half of the Nobel Prize was divided between Heinrich Rohrer and Gerd Binnig for the STM.)

Over the years electron microscopes became more powerful in terms of resolution and by the 1970s atomic structure imaging was routinely possible. By the end of the 1990s sub-Ångstrom resolution was realized following on with the development of commercial aberration correctors. Higher power in terms resolution has been the typical benchmark by which to measure the development of the electron microscope both for the SEM and the TEM; however, with new instrumental advances it now becomes possible for greatly reduced voltage instrument to not only provide the same resolution but rather also improved contrast at the same time.

There are currently multiple texts that address either the general topics in electron microscopy (theory, operation and applications of SEM, TEM or STEM) or more specific subjects, like FIB, ESEM, bio- or polymer microscopy. The intent of this volume is to discuss the rapidly developing and cutting edge field of low voltage microscopy that has only recently become available due to the rapid developments in the electron optics design and image processing. The low voltage techniques are particularly crucial for nanotechnology and research of the surface related phenomena, allowing researches to observe materials as has never been done before. The most recent volume by Scatten and Pawley (eds) published in 2008 focuses solely on the SEM aspects of low voltage observation of biological materials. The volume presented here addresses the recent developments in theory and instrumentation and serves as a practical guide to the current and new microscopists and materials scientists who are active in the field of nanotechnology and biological imaging. The premise of this book is not to cover every single subject under the umbrella of the “low voltage microscopy” but to target principles and practical aspects of this emerging field as it pertains to the imaging techniques in widely used commercial instruments, such as SEM, TEM and STEM.

The opening chapter discusses the general concepts and principles of specimen interaction with electron beam, electron microscope instrumentation and low voltage imaging in SEM and TEM/STEM. The following Chapters (2–5) focus on SEM instrumentation and applications. Chapter 2 (N. Erdman and D.C. Bell) attempts to capture recent developments in SEM instrumentation as they pertain to low voltage microscopy and microanalysis. Chapter 3 is dedicated to development and use of monochromator in SEM (R. Young *et al*.). Chapter 4 discusses practical aspects of sample preparation, imaging and microanalysis for

nanostructured and beam sensitive materials using low voltage. This chapter also references and shows examples of biological imaging with low voltages; however, since there exists a recent volume on this very topic, our goal is to present additional examples.

Chapters 5–7 talk about low voltage applications in TEM and STEM. Chapter 6 by D.C. Bell shows use of aberration corrected and monochromated TEM for imaging of beam sensitive materials down to 40 kV. Krivanek *et al*. show utilization of the “Gentle STEM” technique in Chapter 6 and R.F. Klie discusses STEM imaging and microanalysis of oxide interfaces in Chapter 7.

In the final chapter we have dedicated some discussion to other emerging techniques for low voltage imaging and analysis, such as miniature SEM columns, dedicated low voltage TEM instrumentation as well as utilization of Helium ion microscopy as an alternative to low voltage scanning electron microscopy imaging. Our hope is that current and aspiring electron microscopists, nanotechnology, materials science and biology researches that routinely use electron microscopes for their research will benefit from the theoretical and practical discussions provided in this volume.

We would like to extend our sincere thanks to all the contributors. N. Erdman would like to extend special thanks to A. Laudate of JEOL USA for fruitful discussions and providing some of the excellent graphics used in this volume. The editors would like to thank A. Lazar of Carl Zeiss Microimaging for providing us with relevant micrographs and illustrations. We would also like to thank Professor David Joy for his invaluable insight and advice.

David C. Bell, Cambridge, MA
Natasha Erdman, Peabody, MA

Chapter 1

Introduction to the Theory and Advantages of Low Voltage Electron Microscopy

David C. Bell[1] and Natasha Erdman[2]

[1]School of Engineering and Applied Sciences, Harvard University, USA

[2]JEOL USA Inc., USA

1.1 Introduction

The fundamental aspects of electron microscopy all relate directly to the physics of the interactions between the electron beam and sample. These interactions have been studied extensively since the discovery of the electron by J.J. Thompson in 1897. Energetic electrons are described as “ionizing radiation”—the general term used to describe radiation that is able to ionize or remove the tightly bound inner shell electrons from a material. This is obviously an advantage for electron microscopy in that it produces a wide range of secondary signals such as secondary electrons and X-rays, but is also a disadvantage from the perspective that the sample is “ionized” by the electron beam and possibly structurally damaged, which depending on the accelerating voltage happens in a number of different ways. The

advantages of using a lower accelerating voltage for the electron beam are that the energy is reduced and hence the momentum that *can* be transferred to sample from the electron is also reduced. This, however, has the unwanted effect of reducing the possible emitted signal; although, with recent improvements in detectors, cameras and the use of aberration correctors, the signal to noise and the resolution to produce a final image can not only be maintained but are actually improved.

This chapter will detail the basic theory of electron beam interactions and how it relates to electron microscopy at low voltage. There are, however, distinct differences between the important considerations for low voltage SEM imaging as compared to TEM imaging and these will be detailed in the text.

1.2 Historical Perspective

The early steps in the development of the electron microscope in the 1930s and 1940s by different research groups led ultimately to the development of two distinct groups of instruments: the scanning electron microscope (SEM) and the transmission (or scanning transmission) electron microscope (TEM and STEM). The early microscope designs by Knoll and by Ruska (1933) showed transmission electron images of solid surfaces at 10–16X magnification, which was improved upon by introduction of replica sample preparation technique for TEM observation (Mahl, 1940). As a continuation of his work with Ruska, M. Knoll had designed an electron beam scanner in 1935 (Knoll, 1935) to study targets for the TV camera tubes; this was in essence a predecessor to an SEM, with accelerating voltage up to 4 kV. In 1936 through his contract with the company Siemens, Manfred von Ardenne began development of a scanning transmission electron microscope, mainly to avoid

detrimental effects of chromatic aberration during observation of thick specimens in TEM. The microscope built by von Ardenne had a probe size of 4 nm (von Ardenne, 1937; von Ardenne 1938). The work by von Ardenne, though interrupted by the events of World War II, nonetheless established a theoretical and design background for future SEM and STEM development, particularly regarding understanding of beam/specimen interactions, effect of accelerating voltage on resolution, as well as detector design and positioning within the microscope (von Ardenne, 1985).

From 1938 to 1942, V. Zworykin at RCA headed parallel SEM and TEM development projects that resulted in an SEM instrument with accelerating voltage of 800V (Zworykin *et al.*, 1942). However, poor vacuum in the system significantly impacted the resulting micrographs, and the quality of the recorded images was disappointing with mostly topographic contrast and no meaningful compositional information. These results prompted RCA to discontinue the SEM project and concentrate on the development of the TEM instrument, and led to the development of several commercial instruments. Nonetheless, the work on SEM instrument development continued in Cambridge in early 1950s (McMullan, 1952; McMullan, 2004). R.F.M. Thornley successfully developed the first low voltage SEM (Thornley, 1960) in Oatley's lab at Cambridge University in the early 1960s. By improving upon the existing SEM2 design (Wells, 1957), he was able to obtain 200 nm probe at 1 kV. Prior to that experiment, the SEM was always operated at higher voltages (greater than 6 kV) that allowed only observation of conductive specimens. Thornley's work showed that a surface of alumina ceramic could be imaged at 1.5 kV negating charging artifacts (Thornley, 1960); moreover, he recognized the importance of low voltage in reducing the

charge build up that had caused issues in non-conductive samples.

Over the years, significant improvements in electronics, vacuum and electron column design, as well as detector technology have improved SEM instrument performance to the level where the resolution at 1 kV is on the order of 1–2 nm for high-end field emission systems (see Chapter 2). The recent developments in aberration correction and addition of monochromators to TEM and STEM instruments have further improved their performance for both high and low accelerating voltage applications (see Chapters 6–8).

1.3 Beam Interaction with Specimen—Elastic and Inelastic Scattering

Interaction of a primary electron beam with specimen can generate several different signals (Figure 1.1)—secondary and backscatter electrons, transmitted electrons (if the specimen is sufficiently thin), Auger electrons, characteristic X-rays and photons.

Figure 1.1 Overview of the signals generated when an electron beam interacts with a (relatively) thin specimen. In the case of a thick specimen there are no transmitted electrons and the signal gets absorbed within the material.

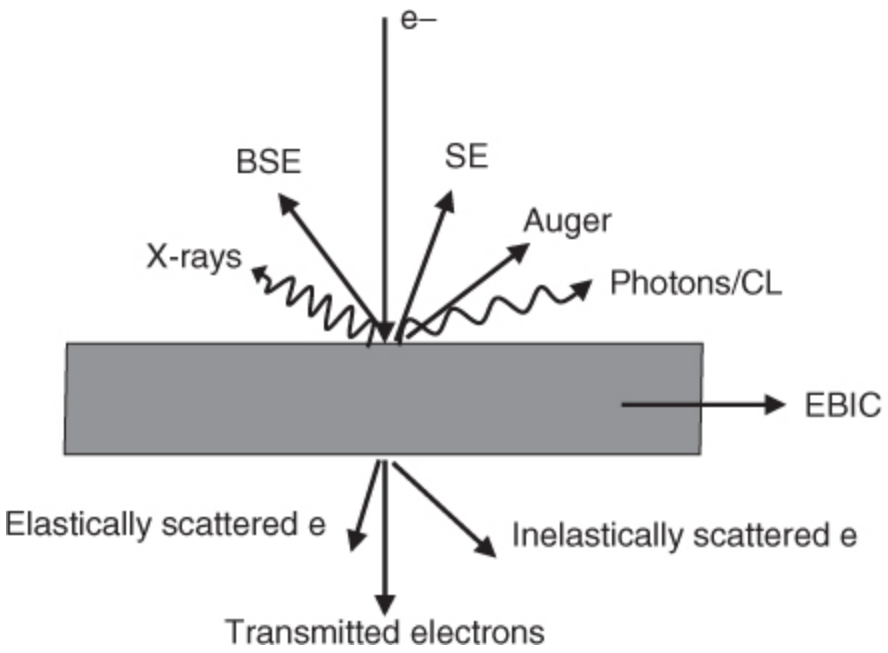

The basic elastic and inelastic scattering processes and electron excitation in materials have a direct influence on the electron range and depth of ionization distribution as well as secondary and backscatter electron emission and the observed contrast in all types of electron microscopes. Particle model of elastic and inelastic scattering processes (based on Bohr atom model) is shown in Figure 1.2(a), while Figure 1.2(b) displays band structure with inelastic processes as well as Auger and X-ray emissions, with respect to different energy levels. Multiple elastic scattering events produce electron backscattering; additional multiple inelastic scattering processes lead to eventual energy loss along the electron trajectories deeper within the material that result in the electrons slowing down and eventually coming to rest. Inelastic scattering is also responsible for the generation of secondary electron signal, Auger electrons, X-rays, electron–hole pairs (semiconductors and insulators), cathodoluminescence and phonon and plasmon production. At lower accelerating voltages, the number of inelastic scattering events decreases; for example, in Si K-shell ionization is no longer possible if accelerating voltage is below 1.84 kV, an effect known as the Duane-Hunt limit.

Figure 1.2 (a) Schematic of elastic and inelastic scattering due to the interaction of electron beam of energy E with an atom. (b) Diagram of inelastic excitations, X-ray, photon and Auger emissions with respect to different energy levels.

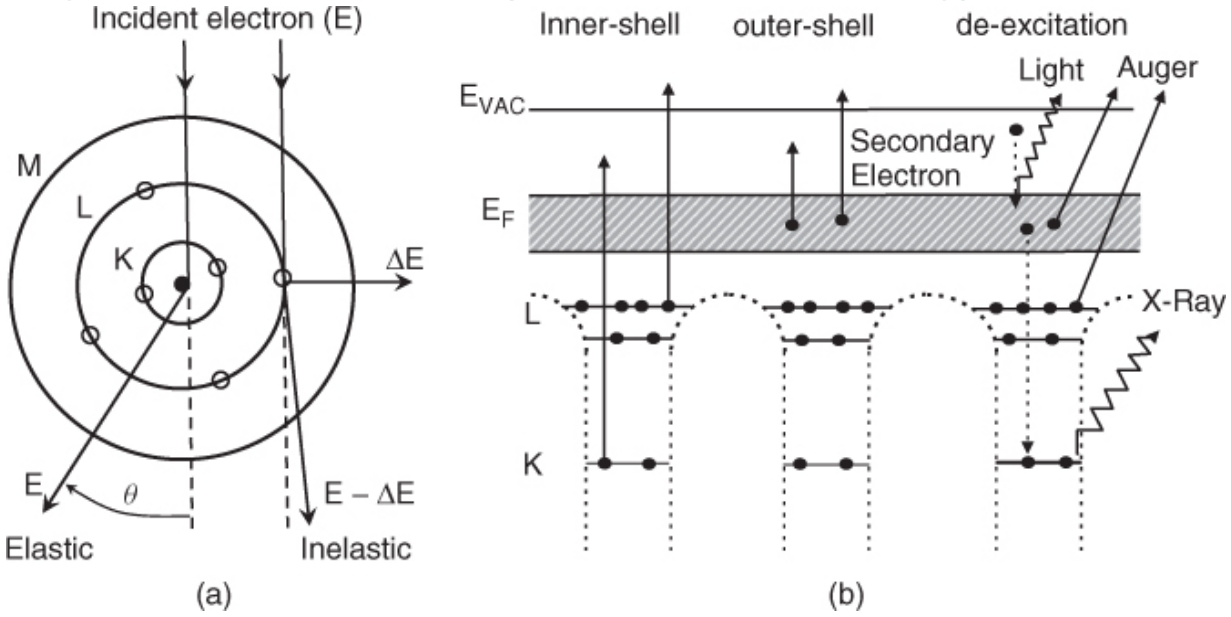

Understanding of the elastic and inelastic scattering processes can additionally serve as a basis for modeling of beam/specimen interactions (particularly for SEM imaging and analysis) via Monte–Carlo simulations to investigate electron trajectories in materials and calculate theoretical secondary and backscatter electron spatial distributions based on the specimen position under the beam (angle), accelerating voltage and the material type. Several different programs are available for these types of calculations; more specifically Casino (Drouin *et al.*, 2007; also http://www.gel.usherbrooke.ca/casino/index.html) has been written particularly with a focus on low voltage imaging and analysis.

The quantum mechanical properties of electron are such that the electron has a wavelength defined by de Broglie relationship:

$$\lambda = \frac{h}{p} = \frac{h}{\sqrt{2m_0 E}} \quad \textbf{1.1}$$

where h is the Planck constant, m_0 is the rest mass of the electron and E the accelerating voltage. However, since electrons in the electron microscope are moving at high speeds defined by the accelerating voltage of the electron gun this equation needs to be rewritten be become the relativistic version (where E_0 is the rest energy):

$$\lambda = \frac{hc}{\sqrt{2EE_0 + E^2}} \quad \textbf{1.2}$$

This means that for a 200 kV electron we have a wavelength of 2.5 pm, but for a 40 kV electron the wavelength becomes nearly three times as large at 6 pm. If we plot wavelength as a function of accelerating voltage, we see that the wavelength increases exponentially as the accelerating voltage decreases below about 20 kV (Figure 1.3). For an SEM operating at 1 kV the wavelength becomes 39 pm, still a small value but a significantly larger wavelength as compared to, for example, 40 kV. The limiting factor for resolution of electron microscope is ultimately the electron wavelength; moreover, the actual working resolution of electron microscopes is directly limited by the lens aberrations present, as detailed later in this chapter. As Figure 1.1 shows, there is a variety of different possible signals generated by the interaction of primary beam with the specimen and to start with we separate these processes based on the differences in the scattering cross section between elastic and inelastic scattering.

Figure 1.3 Dependence of electron wavelength on the accelerating voltage.

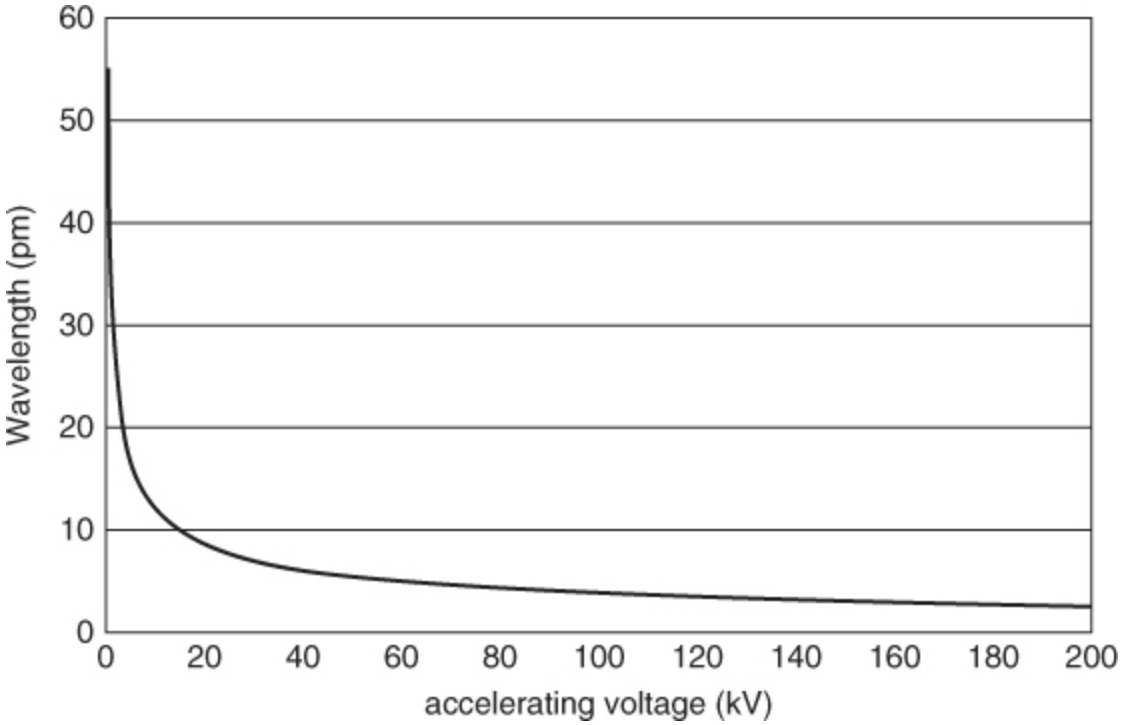

1.3.1 The Scattering Cross Section

The probability of an incident electron being scattered by a given atom per unit solid angle Ω is represented by the differential scattering cross section $d\sigma/d\Omega$ that is a function of the scattering angle θ (Figure 1.4). Interaction of the primary beam electrons with the attractive nucleus Coulomb potential results in elastic scattering processes, with change in a primary electron beam trajectories through angle θ, but negligible energy loss (on the order of meV). For elastic scattering, the cross section is given by:

$$\frac{d\sigma}{d\Omega} = |f(\theta)|^2 \quad \textbf{1.3}$$

where f is the scattering factor, which is a function of the scattering angle θ. Assuming a single scattering within each atom (the first Born approximation), scattering factor is proportional to the tree dimensional Fourier transform of the atomic potential $V(r)$. The elastic scattering cross section

can also be expressed as a function of an elastic scattering factor *F(q)*:

$$\frac{d\sigma}{d\Omega} = \frac{4}{a_0^2 q^4} |F(q)|^2 = \frac{4\gamma^2}{a_0^2 q^4} |Z - f_x(q)|^2 \quad \textbf{1.4}$$

where $f_X(q)$ is the atomic scattering factor of an incident photon and equals the Fourier transform of the electron density within the atom; $a_0 = 4\pi\epsilon_0^2/m_0e^2 = 0.529 \times 10^{-10}$ m is the Bohr radius, $\gamma = (1-v^2/c^2)^{-1/2}$ is a relativistic factor and $q = 2k_0\sin(\theta/2)$ is the scattering vector. The incident electrons are scattered by the entire electrostatic field of the atom (as opposed to X-rays that interact only with the atomic electrons), hence the inclusion of the atomic number (or nuclear charge) Z in Equation 1.4.

Figure 1.4 Electron scattering as a function of scattering angle θ. Superposition of an incident plane wave with amplitude $\psi = \psi_0\exp(2\pi i k_0 z)$ and a spherical scattered wave with amplitude $\psi_{SC} = \psi_0 f(\theta)\exp(2\pi i k_0 r)/r$.

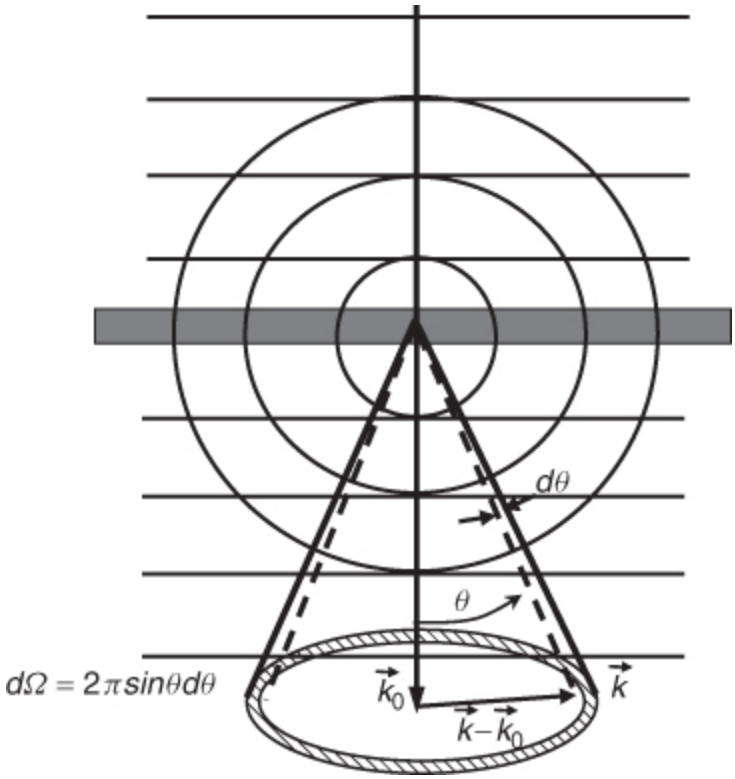

The relatively simple Rutherford scattering model (Rutherford, 1911) has been widely used in the past to describe elastic scattering of charged particles based on the unscreened electrostatic field of a nucleus. Setting the electronic term, $f_X(q)$, in Equation 1.4 to zero, the differential cross section becomes:

$$\frac{d\sigma}{d\Omega} = \frac{4}{a_0^2 q^4} Z^2 \gamma^2 \quad \textbf{1.5}$$

The above equation is a reasonable approximation for light elements at large scattering angles (and has been often employed for modeling of high kV SEM imaging); however, at small scattering angles the equation breaks down, mainly due to the fact that the nuclear screening is not taken into account.

The nuclear screening can be incorporated via an expression for nuclear potential attenuated exponentially as a function of distance from the nucleus (r):

$$V(r) = \left(\frac{Ze}{4\pi\varepsilon_0 r}\right)\exp\left(-\frac{r}{r_0}\right) \quad \textbf{1.6}$$

where r_0 is the screening radius. The elastic scattering cross section then becomes:

$$\frac{d\sigma}{d\Omega} = \frac{4\gamma}{a_0^2}\left(\frac{Z}{q^4 + r_0^2}\right)^2 \approx \frac{4\gamma^2 Z^2}{a_0^2 k_0^4}\frac{1}{\left(\theta^2 + \theta_0^2\right)^2} \quad \textbf{1.7}$$

where $\theta_0 = (k_0 r_0)^{-1}$ and $r_0 = a_0 Z^{-1/3}$ (Lenz, 1954). The model in Equation 1.7 provides a quick estimate of the angular dependence of scattering; however, there are more sophisticated methods for calculating cross sections that take into account relativistic effects (for example Mott scattering cross section), and are particularly relevant at low incident energies.

A more accurate treatment of the elastic scattering cross section is achieved by taking into account relativistic quantum mechanics based on the Dirac equation. For example, Mott scattering cross-section (Mott, 1932; Mott and Massey, 1949; Reimer, 1993) incorporates the effect of spin-orbit coupling of electrons and thus differs from Rutherford scattering. Mott cross-section is especially applicable when describing beam-specimen interactions in the case of low voltage SEM observation. Mott cross-section is a quite complex function of primary electron energy, atomic number and scattering angle and several empirical models based on tabulated values have emerged and are being currently used in various beam/specimen interactions simulation programs (Czyzewski *et al.*, 1990; Gauvin and Drouin, 1993; Browning *et al.*, 1995; Hovington *et al.*, 1997).

Inelastic scattering is typically described as scattering events that result in energy loss of ΔE for the primary beam electrons through energy transfer to the atoms in the sample through interaction with either outer or inner shell

atomic electrons; however, inelastic scattering does not significantly alter the electron trajectory.

The differential cross section for inelastic scattering can be written as (Reimer and Kohl, 2008):

$$\frac{d\sigma_i}{d\Omega} = \frac{4\gamma^2 Z}{a_0^2 q^4}\left(1 - \frac{1}{\left[1+(qr_0)^2\right]^2}\right) \quad \textbf{1.8}$$

in which the scattering vector q is given by:

$$q^2 = k_0^2\left(\theta^2 + \overline{\theta}_E^2\right) \quad \textbf{1.9}$$

where $k_0 = 2\pi/\lambda$ is the magnitude of the incident electron wave vector, θ is the scattering angle, $\overline{\theta}_E = \overline{E}/\gamma m_0 v^2$ is the angle associated with the mean energy loss of $\overline{E}$. The above two expressions can be combined to give the expression for inelastic scattering cross section as a function of the scattering angle (Colliex and Mory, 1984):

$$\frac{d\sigma_i}{d\Omega} = \frac{4\gamma^2 Z}{a_0^2 k_0^4}\frac{1}{\left(\theta^2 + \overline{\theta}_E^2\right)^2}\left\{1 - \left[1 + \frac{\overline{\theta}_E^2}{\theta_0^2} + \frac{\theta^2}{\theta_0^2}\right]^{-2}\right\} \quad \textbf{1.10}$$

Figure 1.5 illustrates angular distribution of elastic and inelastic scattering cross sections calculated in carbon at an accelerating voltage of 100 kV showing how the scattering cross section decreases rapidly from zero degrees, interestingly of note is how the inelastic scattering starts higher than elastic and then drops off more rapidly than the elastic. For more detailed discussion and analysis of differential cross sections see for example Egerton (2011) and Reimer and Kohl (2008).

Figure 1.5 Angular dependence of elastic (dashed line) and inelastic (solid line) cross sections for carbon at accelerating voltage of 100 kV.

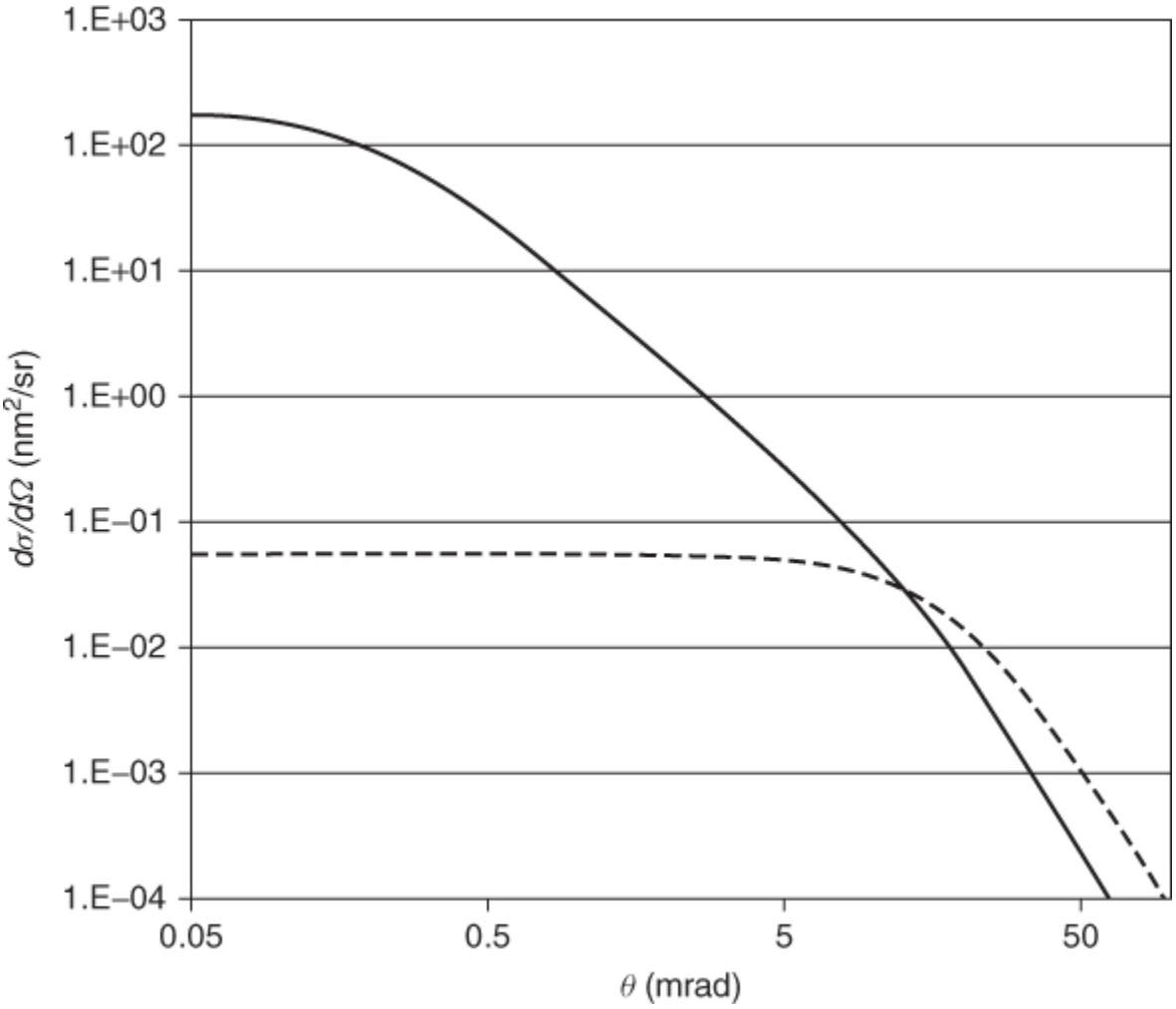

1.3.2 Effects of Specimen Damage

Although elastic and inelastic scattering processes are essential for imaging and spectroscopy in electron microscope, they are also responsible for the electron beam induced specimen damage and alteration. The two most common damage mechanisms are termed radiolysis and knock-on damage.

Knock-on damage occurs when the incident electron energy is higher than the atomic sputtering threshold energy (Mott, 1932; Hobbs, 1979), thus inducing either an atom removal from its site or sputtering from the surface.

The maximum energy that can be transferred to an atom during a collision is:

$$E_{\max} = \frac{2E(E + 2m_0c^2)}{M_0c^2} \quad \textbf{1.11}$$

where E in the incident electron energy, M_0 is the mass of the atom, and m_0c^2 is the rest energy of the electron. Equation 1.11 describes the threshold energy (E_{th}) needed for incident electrons to displace or sputter atoms.

Radiolysis damage is induced by converting the exciton energy generated by incident beam interaction with specimen into momentum and thus creating atomic displacements in the analyzed material (Hobbs and Pascucci, 1980; Pascucci, 1983). In order for radiolysis to occur the exciton energy should be larger than the energy needed for atomic displacement, and the exciton relaxation time should be sufficiently long (≥1 ps) such that the bonding instabilities can be induced by mechanical relaxation of the atoms. Radiolysis processes are common in materials like organic compounds, silicates, halides and ice (Hobbs, 1979).

Some recent experimental observations and theoretical predictions suggest that below incident energies of 70 kV the damage is mainly radiolitic; whereas at incident energies above 200 kV the knock-on damage and material sputtering will be dominant (Ugurlu *et al.*, 2011). Therefore, TEM and STEM imaging at low voltages should substantially reduce knock-on damage.

1.4 Instrument Configuration

1.4.1 Scanning Electron Microscope

The scanning electron microscope (SEM) operates by rastering a fine electron probe (few nm in size) over a region of the specimen. Typical scanning electron microscope configuration is shown in Figure 1.6(a). Contemporary SEM instruments usually operate between few tens of volts and 30 kV, and are traditionally used for examination of bulk materials, though very thin specimens can be examined in transmission mode as well. The spatial resolution of the instrument is characterized by the electron probe diameter that can be achieved with the combination of electron source size and the lens configuration; however, the beam/specimen interaction volume further limits the instrument resolution. The instrument can collect (depending on the detector configuration) secondary, backscatter and transmitted electron signals. Moreover, signals like X-ray emission (EDS and WDS), cathodoluminescence (CL), electron backscatter diffraction (EBSD) and electron beam induced current (EBIC) can be detected.

Figure 1.6 Simplified schematic cross-sections of an (a) SEM, (b) TEM and (c) STEM instrument.